Dressed-photon–phonon creation probability on the tip of a fiber probe calculated by a quantum walk model

M. Ohtsu[1], E. Segawa[2], K. Yuki[3], and S. Saito[4]

[1]Research Origin for Dressed Photon,3-13-19 Moriya-cho, Kanagawa-ku, Yokohama, Kanagawa 221-0022, Japan

[2]Yokohama National University, 79-8 Tokiwadai, Hodogaya-ku, Yokohama, Kanagawa 240-8501, Japan

[3]Middenii, 3-3-13 Nishi-shinjuku, Sinjuku-ku, Tokyo 160-0023, Japan

[4]Kogakuin University, 2665-1, Nakano-machi, Hachioji, Tokyo 192-0015, Japan

Abstract

To study the probability of a dressed-photon–phonon (DPP) created on the tip of a fiber probe based on a quantum walk (QW) model, the creation probability of the DPP at the apex of a triangle is numerically calculated by substituting several values of mathematical and physical parameters. Two cases are dealt with: One is the case in which the DPP energy does not dissipate from the slope of the triangular lattice; and the other is the case in which the DPP energy dissipates. Sufficiently high accuracy of the approximation was obtained when the number of sites on the base of the triangle was larger than 51. The probability of DPP creation at the apex of the triangle was larger in the case without DPP energy dissipation at the slope of the triangle than that in the case with dissipation; furthermore, it was larger for a triangle with a larger apex angle. The derived results were in agreement with experimental results.

1. Introduction

A dressed photon (DP) is a quantum field that is created as the result of an interaction between photons and excitons (pairs consisting of electrons and positive holes) in a nanometer-sized particle (NP). After the DP is created on an NP, it hops to adjacent NPs, where it creates a phonon. The created phonon interacts with the DP to form a new quantum field, which is called a dressed-photon–phonon (DPP) [1]. A quantum walk (QW) model was employed to analyze the tempo-spatial behavior of the DPP energy transfer [2].

In the present paper, the probability of DPP creation on the tip of a fiber probe was numerically calculated based on the QW model, and the calculated results were compared with experimental ones. The results of preliminary calculations have been reported by ref. [3]. In Section 2, the purpose and method of calculation are reviewed. In Section 3, the profile of the fiber probe is approximated by a right-angled isosceles triangle, in which a part of a square lattice is embedded. The dependence of the calculated results on the number of the sites in the triangle is discussed. In Section 4, the fiber probe is approximated by an equilateral triangle, in which a part of a triangular lattice is embedded. The dependence of the probability of DPP creation on the apex angle of the fiber probe is discussed by comparing the calculated results with those in Section 3. Section 5 summarizes

1

the results derived in the present paper.

2. Purpose and method

The present calculations are based on a two-dimensional QW model for simplicity. Figure 1 shows a right-angled isosceles triangle, in which a part of a square lattice is embedded. Here, the number of the sites on the base of the triangle is n, and this triangle is expressed as $T_R(n)$. This figure schematically explains that, by applying input signals to all the sites on the base of the $T_R(n)$, DPs are created and transferred to the adjacent sites. During this transfer, DPPs are created by the DP–phonon interaction. These DPPs transfer through the $T_R(n)$ and finally reach its apex (the tip of the fiber probe). This apex is assumed to be a sink from which the DPP energy is dissipated. This paper calculates the creation probability P of the DPP at this sink. It should be pointed out that each site in the $T_R(n)$ has four nearest-neighbor sites located along the $\pm x$-, and $\pm y$-axes originated from the embedded square lattice. This means that the DPP energy transfers from/to these four sites.
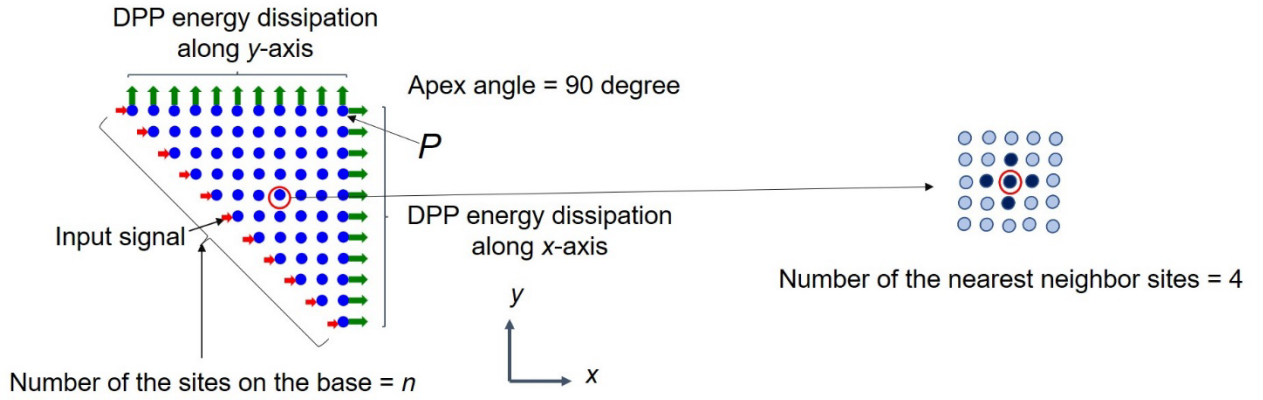

Fig. 1 A right-angled isosceles triangle $T_R(n)$, in which a part of a square lattice is embedded.

Three parameters are used for the calculation:

(1) Mathematical parameter ξ:

To cover a broader range of mathematical discussions based on the QW model, a phase angle ξ is introduced to the real-valued unitary matrix in eq. (6) of ref. [2]:

$$U = \begin{bmatrix} \varepsilon_+ & J & \chi \\ J & \varepsilon_- & \chi \\ \chi & \chi & \varepsilon_0 \end{bmatrix}. \qquad (1)$$

As a result, U is replaced by a complex-valued matrix

$$U(\xi) = \exp(i\xi)U . \qquad (2)$$

Here, ξ is regarded as a mathematical parameter.

(2) Physical parameter χ/J:

Since the quantities J and χ in eq. (1) represent the energies of the DP-hopping to the adjacent

NP (an atom in the fiber probe) and of the DP–phonon interaction, respectively, their ratio χ/J is

regarded as a physical parameter. The value of χ/J may be fixed to 1 for simplicity, as was

recommended in ref. [2]. However, to cover a broader range of physical discussions, the present paper

employs a wider range of values, i.e., $0.1 \le \chi/J \le 10$.

(3) Parameter n for numerical calculation:

The total number of sites increases as the number n of sites on the base of the $T_R(n)$ increases.

Since this increase can improve the accuracy of approximating the fiber probe by the $T_R(n)$, n is

regarded as a parameter for the numerical calculation.

The probability P is numerically calculated by substituting several values of ξ and

χ/J into eqs. (1) and (2). The parameter n was fixed to $5-61$ due to the limit of the computation

time.

Two cases are dealt with: One is the case in which the DPP energy does not dissipate from the

slope of the $T_R(n)$. The other is the case in which the DPP energy dissipates. For the former case, the

tempo-spatial evolution equation at the slope is given by eq. (12a) in ref. [2], which is

$$\vec{\psi}_{t+1,(x,y)}^{\Leftrightarrow} = \sigma P_-^{\Updownarrow} \vec{\psi}_{t,(x,y)}^{\Updownarrow} + P_-^{\Updownarrow} \vec{\psi}_{t,(x+1,y)}^{\Updownarrow} + P_0^{\Updownarrow} \vec{\psi}_{t,(x,y)}^{\Updownarrow} . \tag{3}$$

Here, the matrix σ represents the DPP energy reflection at the slope. For the latter, the equation, given by eq. (10b) in ref. [2], is

$$\vec{\psi}_{t+1,(x,y)}^{\Updownarrow} = P_+^{\Leftrightarrow} \vec{\psi}_{t,(x,y-1)}^{\Leftrightarrow} + P_-^{\Leftrightarrow} \vec{\psi}_{t,(x,y+1)}^{\Leftrightarrow} + P_0^{\Leftrightarrow} \vec{\psi}_{t,(x,y)}^{\Leftrightarrow} . \tag{4}$$

3. Dependence on number of sites

Figure 2 shows an example of the calculated temporal behavior of the value of P. After the input signals are applied to all the sites on the base of the $T_R(n)$ simultaneously, the value of P increases with time and reaches a stationary value. Recent QW theoretical studies have found that the temporal behavior of the value of P on a complete graph exhibits pulsation prior to converging to the stationary value [4]. They have also found that the pulsation interval T_p is proportional to $\pi\sqrt{2N}$.

Furthermore, the time T_s required to converge to the stationary value is proportional to $N\log N$. Here, N is the total number of sites in a lattice, that is equal to $n(n+1)/2$ in the case of the RIT lattice. The profile of the curve in Fig. 2 qualitatively agrees with the results of these theoretical studies. The present paper discusses the dependence of the stationary value of P on the parameters in eqs. (1) -(4).
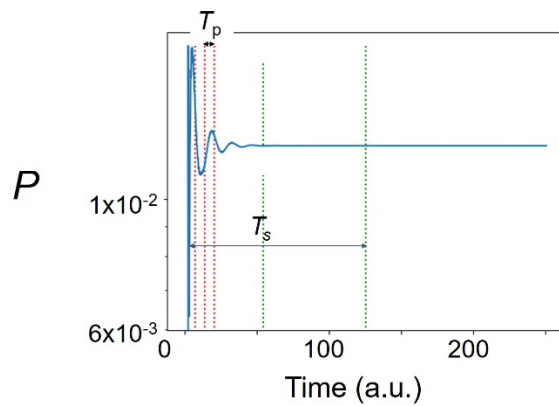

Fig. 2 An example of the calculated temporal behavior of the value of P.

Figure 3 shows the external forms and cross-sectional structures of fiber probes [5]. The DPP energy dissipates from the taper of the fiber probe. This corresponds to radiating scattered light from

4

the taper. In order to avoid this radiation, an opaque metallic film is coated on the taper to realize a high-efficiency fiber probe (Fig. 3(a)). This is the prototype of devices that are now popularly used. Figure 3(b) is a basic fiber probe without a metallic film coating, resulting in DPP energy dissipation from the taper. This is a primitive device that was used only in the early stages of DP science. Corresponding to Figs. 3(a) and (b), numerical calculations are carried out for the two cases below.
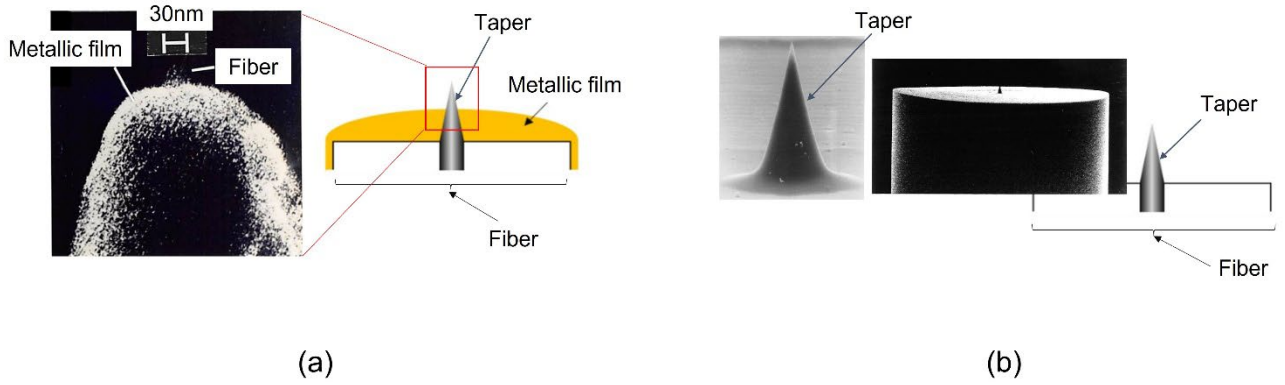

(a)   (b)

Fig. 3 External forms and cross-sectional structures of the fiber probes.

(a) A high-efficiency fiber probe with an opaque metallic film on the taper. (b) A basic fiber probe.

Case 1: Without DPP energy dissipation

Figure 4 shows the calculated results of the dependence of the probability P on the parameters ξ and χ / J. The parameter n was fixed to 5, 11, 21, 31, 41, 51, and 61 in Figs. 4(a)-(g). The values of P at $\chi / J = 1$ (as was recommended in ref. [2]) are extracted from these figures, and their dependences on ξ are shown in Figs. 5(a) – (g). The curves in these figures show a lot of bumps that are attributed to interference in the $T_R(n)$ originating from reflection at the slope.

Figure 5 shows that the value of P takes the maximum $P_{\max}$ at $\xi = 67.5$ degree. This value of ξ is equal to $(3/8)\pi$. The reason why the rational number 3/8 appears here should be studied in

the future. Figure 6 shows the dependence of this maximum P_{max} on n. This figure shows that P_{max} asymptotically approaches a constant value of 3×10^{-1} as n increases, from which it was confirmed that a sufficiently high accuracy of approximation for the numerical calculation was obtained when $n \geq 51$. Figure 7 shows the dependence of the ratio between the maximum P_{max} and the minimum

P_{min} (of the curves in Fig. 5) on n. The ratio in this figure also shows an asymptotic approach to a constant value, from which it was confirmed again that sufficiently high accuracy was obtained when $n \geq 51$.
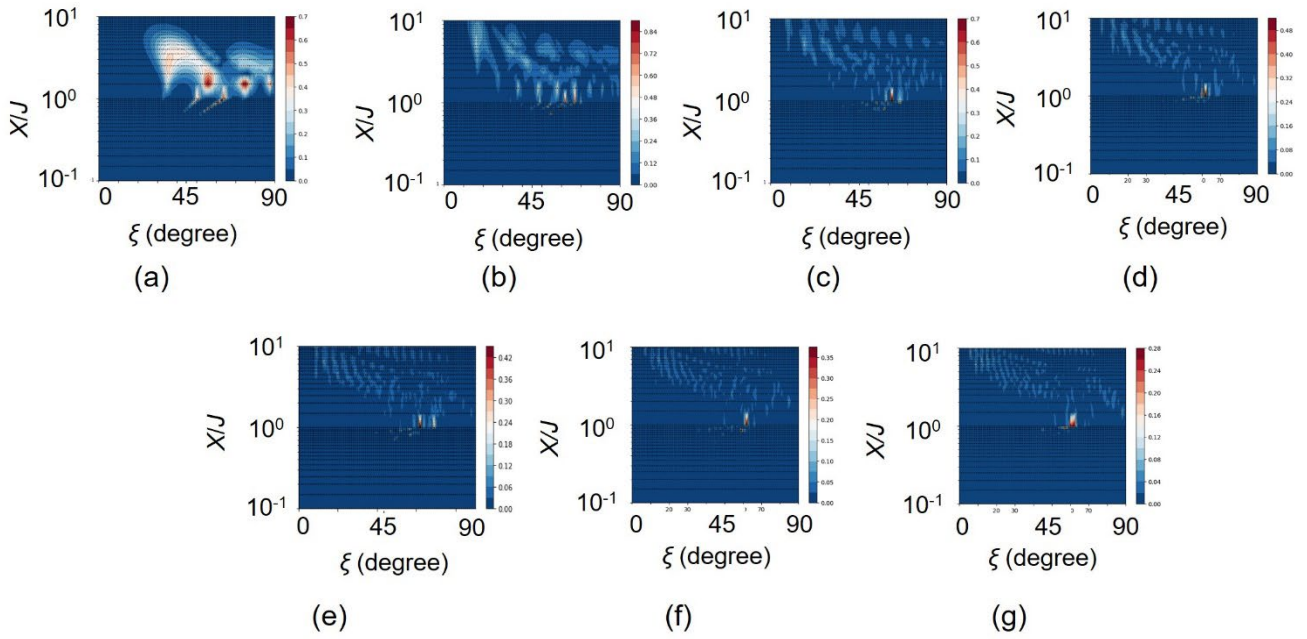
Fig.4 Dependence of P on ξ and χ / J in the case without DPP energy dissipation.

n is 5 (a), 11 (b), 21 (c), 31 (d), 41 (e), 51 (f), and 61 (g).
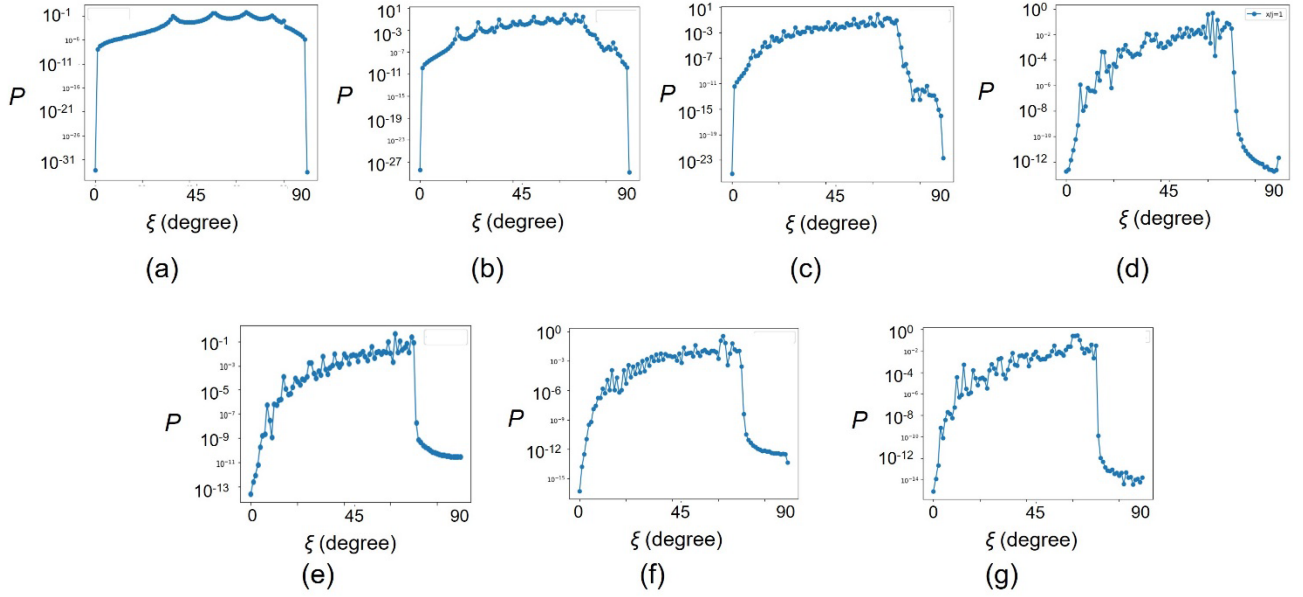
Fig.5 Dependence of P on ξ at $\chi/J=1$.

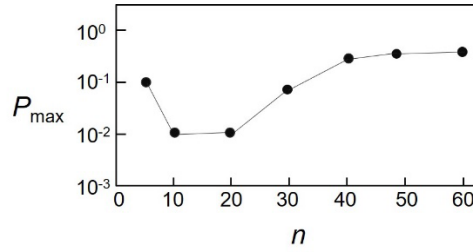n is 5 (a), 11 (b), 21 (c), 31 (d), 41 (e), 51 (f), and 61 (g).

Fig. 6 Dependence of the maximum P_{max} on n.
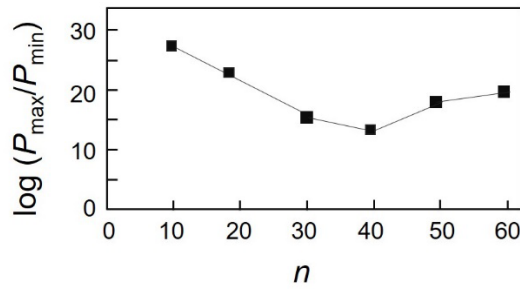

Fig. 7 Dependence of the ratio between the maximum P_{max} and minimum P_{min} on n.

Case 2: With DPP energy dissipation

Figure 8 shows the calculated results of the dependence of P on ξ and χ/J. In Figs. 8(a)-(g), n is fixed to 5, 11, 21, 31, 41, 51, and 61. Crescent-shaped red belts are seen in the upper right parts of these figures, in which the value of P is very large in comparison with those outside the red belts. It takes the maximum value at the position $\square$. The origin of these red belts is attributed to intrinsic properties of the QW or dispersive features of the phonon energy. The values of P show irregular variations and abrupt increases in the red belts and at their rims. The value of χ/J at $\square$ increases with the increases of n, as is shown by Fig. 9. It increases to $\chi/J \gg 1$, which means that the value of P at $\chi/J = 1$ (as was recommended in ref.[2]) does not vary irregularly with ξ.
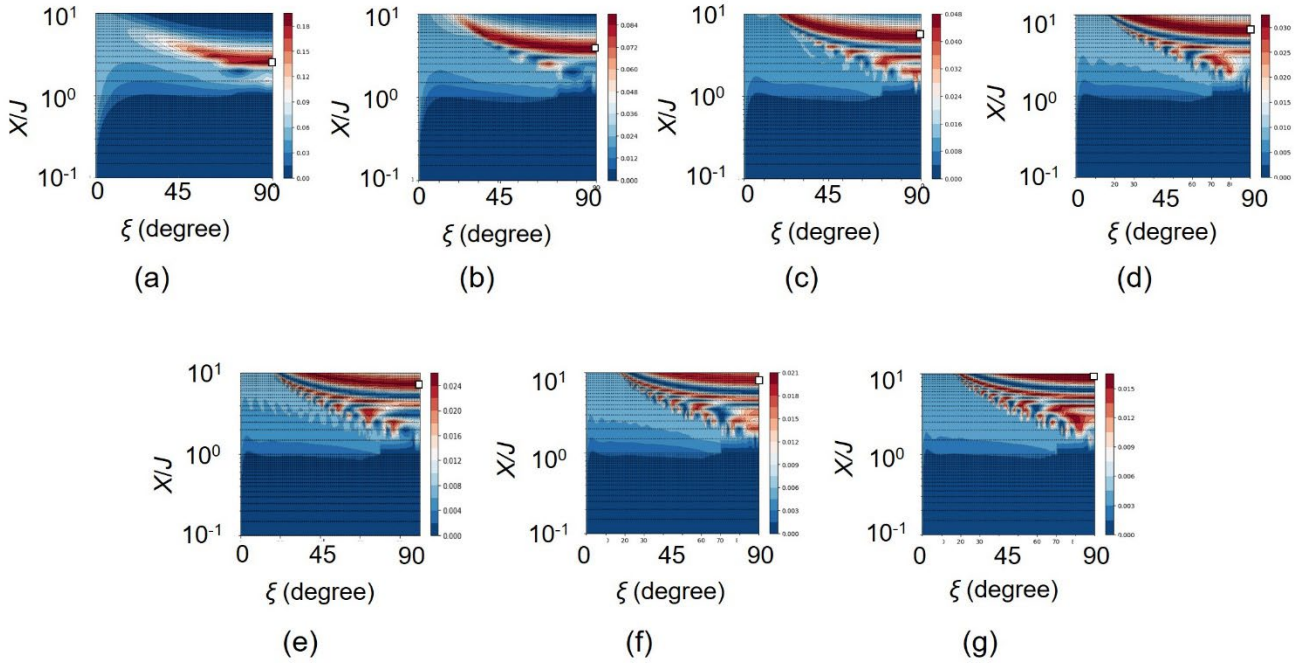

Fig.8 Dependence of P on ξ and χ/J in the case with DPP energy dissipation.

n is 5 (a), 11 (b), 21 (c), 31 (d), 41 (e), 51, (f), and 61 (d). $\square$ is the position for P_{max} in the red belt.
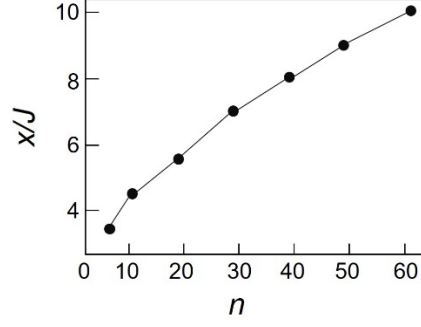
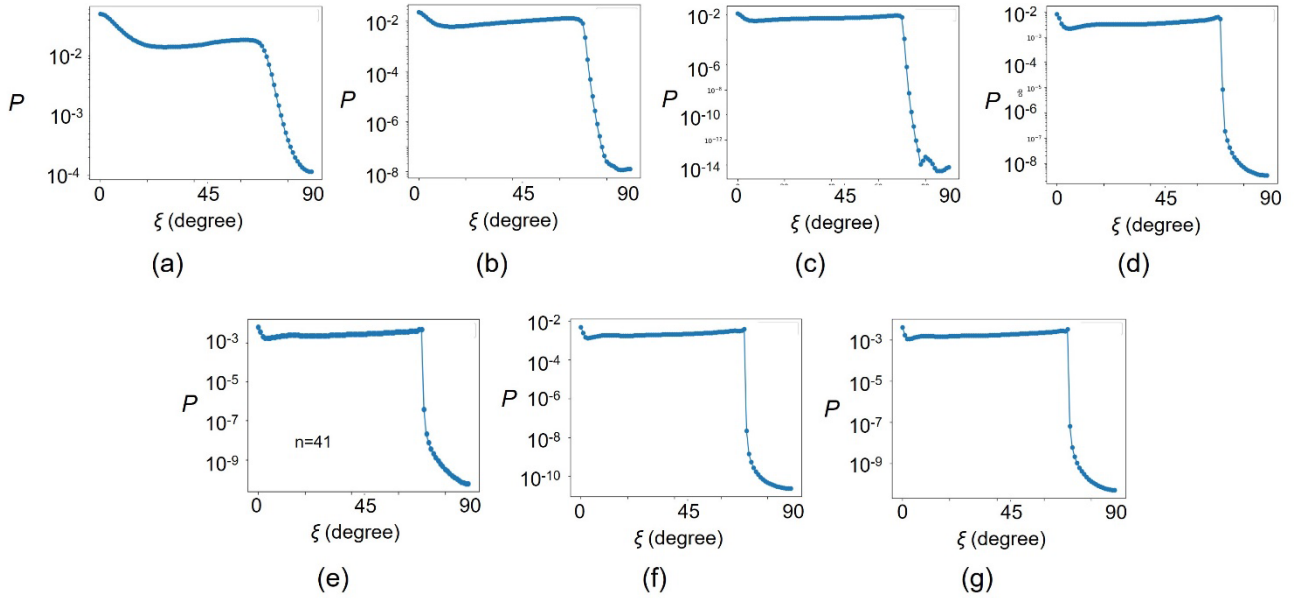Fig. 9 Dependence of χ/J on n at the position □ in Fig. 8.

Fig. 10 Dependence of P on ξ at $\chi/J=1$.

n is 5 (a), 11 (b), 21 (c), 31 (d), 41 (e), 51, (f), and 61 (d).

The value of P at the area isolated from the red belt is now evaluated for studying its regular and smooth variations. For this evaluation, χ/J is fixed to 1 (as was recommended in ref. [2]), and the dependence of on ξ and n is derived as shown by Fig. 10. In contrast to Fig. 5, no bumps are seen on the curves in this figure, which indicates that no interference takes place in the RIT lattice. This is due to the absence of reflection at the slope.

As in Case 1, the value of P in Fig. 10 takes the maximum P_{max} at $\xi=67.5$ degree. Figure

11 shows the dependence of P_{max} on n. This figure shows that the value of P_{max} asymptotically approaches a constant value as n increases, from which it was confirmed that sufficiently high accuracy of approximation was obtained when $n \geq 51$, as in Case 1 above. The value of P_{max} was 3 $\times 10^{-3}$ for $n \geq 51$, which is 10^{-2} times that in Fig. 6. This indicates that it is effective to suppress DPP energy dissipation (Case 1) at the slope of the RIT lattice to increase the probability of DPP creation. This indication is compatible with experimental results in which the taper of a fiber probe is coated with an opaque metallic film to suppress dissipation and to increase the DPP creation efficiency at the tip of the fiber probe (refer to Fig. 3(a)).
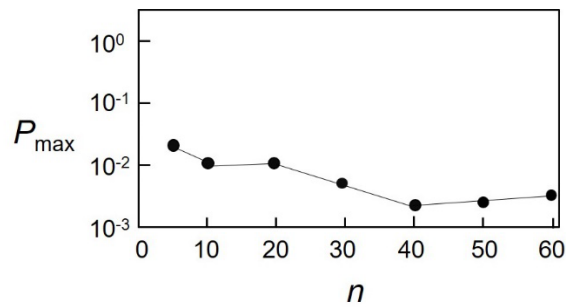

Fig. 11 Dependence of the maximum P_{max} on n.

Figure 12 shows the dependence of the ratio between the maximum P_{max} and the minimum P_{min} (of the curves in Fig. 10) on n. The curve in this figure also shows an asymptotic approach to a constant value, from which it was confirmed that sufficiently high accuracy was obtained when $n \geq 51$.
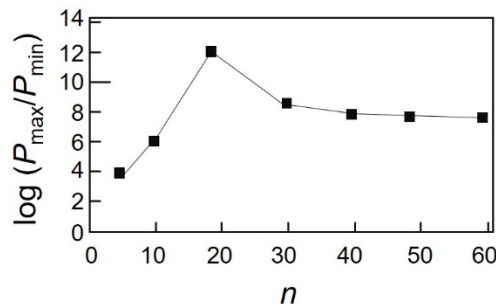

Fig. 12 Dependence of the ratio between the maximum P_{max} and minimum P_{min} on n.

4. Dependence on apex angle of fiber probe

Experimental studies have found that the value of P was smaller for smaller apex angles [6]. Unlike the 90 degree apex angle of the $T_R(n)$ in Section 3, this section deals with a triangle with a smaller apex angle, i.e., an equilateral triangle $T_E(n)$ (apex angle of 60 degrees), as an example, as is shown in Fig. 13. The calculated results are compared with those in Section 3.
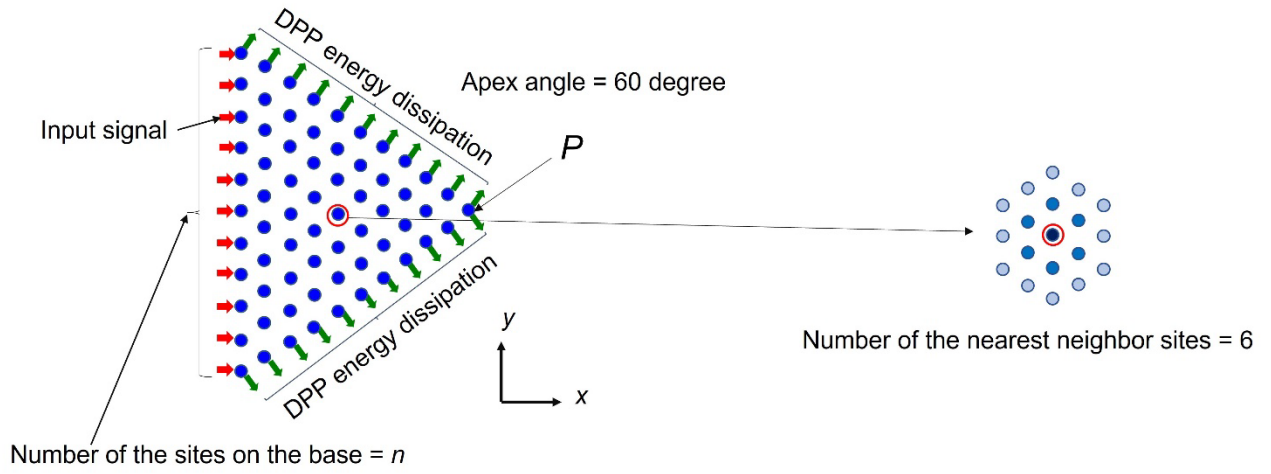

Fig. 13 An equilateral triangle $T_E(n)$, in which a part of a triangular lattice is embedded.

Being different from the $T_R(n)$, each site in the $T_E(n)$ in Fig. 13 has six nearest-neighbor sites located along the directions of the $e^{\pm i\pi/6}x$-, $e^{\pm i5\pi/6}x$-, and $\pm y$-axes originated from the embedded triangular lattice. The DPP energy transfers from/to these six sites. By noting the number of these nearest-neighbor sites, the tempo-spatial evolution equation for the $T_E(n)$ was derived by modifying that for the $T_R(n)$, and the probabilities P were calculated for the cases without and with DPP energy dissipation.

Case 1: Without DPP energy dissipation

Figure 14 shows the dependence of P on ξ and on χ/J. Figure 15 shows the dependence of P in Fig. 14 on ξ at $\chi/J=1$. A lot of bumps are seen on the curves in this figure, which are attributed to interference in the triangular lattice, originating from the reflection at the slope, as were seen in Fig. 5. It was confirmed that these curves are symmetrical about $\xi=60$ degree. Furthermore, the value of P in these figures takes the maximum P_{max} at $\xi=60$ degree $(=(1/3)\pi)$.
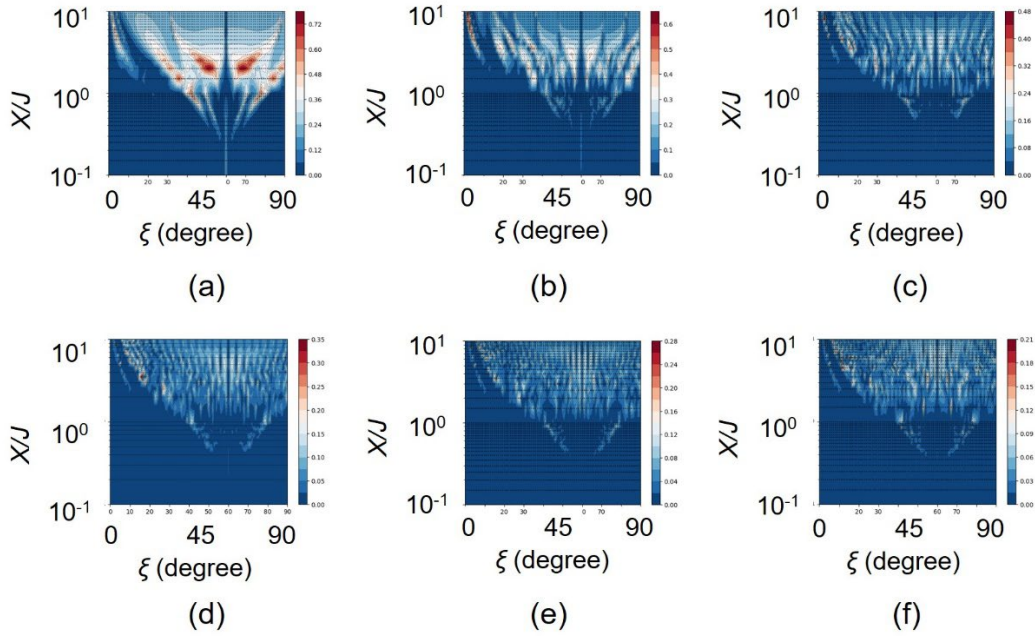

Fig. 14 Dependence of P on ξ and χ/J in the case with DPP energy dissipation.

(a) $n=5$, (b) 11, (c) 21, (d) 31, (e) 41, and (f) 51.

Figure 16 shows the dependence of P_{max} on n, in which the value at $n=61$ was not obtained due to the upper limit of the computation time. This figure shows that the value of P_{max} asymptotically approaches a constant value as n increases, from which it was confirmed that sufficiently high accuracy of approximation was obtained when $n \geq 51$. Figure 17 shows the

dependence of the ratio between the maximum P_{max} and the minimum P_{min} (of the curves in Fig. 15) on n. The ratio in this figure also shows an asymptotic approach to a constant value, from which it was confirmed again that sufficiently high accuracy of approximation was obtained when $n \geq 51$.
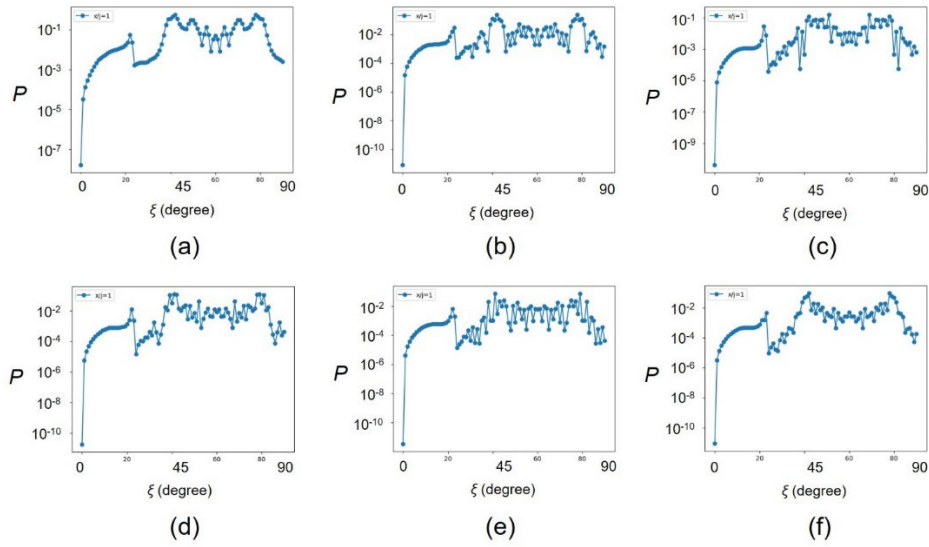

Fig. 15 Dependence of P on ξ at $\chi / J = 1$ in Fig. 14.

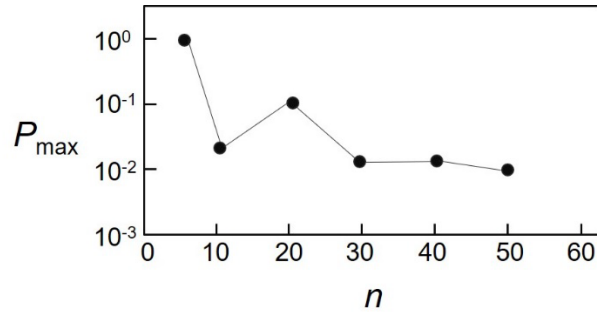(a) $n = 5$, (b) 11, (c) 21, (d) 31, (e) 41, and (f) 51.

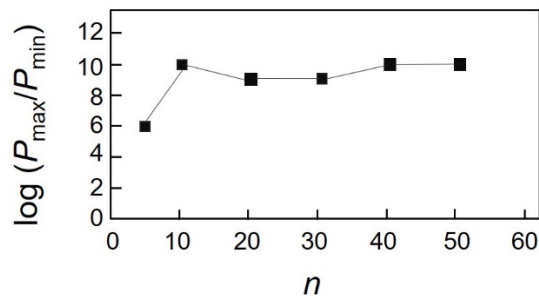Fig. 16 Dependence of P_{max} on n in Fig. 14.

13

It is found that the value of $P_{\max}$ in Fig. 16 is 1×10^{-2} for $n \geq 51$, which is smaller than the value 3×10^{-1} in Fig. 6. This smaller value indicates that the efficiency of DPP creation is lower for a smaller apex angle of the fiber probe, which is in agreement with the experimental results [6], as was described at the beginning of this section.

Case 2: With DPP energy dissipation

Figure 18 shows the dependence of P on ξ and on χ / J. A red belt is seen in this figure, as was the case in Fig. 8, in which the value of P is very large in comparison with those outside the belts. The value of P is integrated over the range $0 \leq \xi \leq 90.0$ degree, and Fig. 19 shows the dependence of χ / J on n at which the integrated value of P takes the maximum in the red belt, indicating that χ / J takes a constant value as n increases. Furthermore, this value of χ / J is larger than 2, which means that the value of P at $\chi / J = 1$ (as was recommended in ref. [2]) does not suffer any effects from the red belt.

(a)

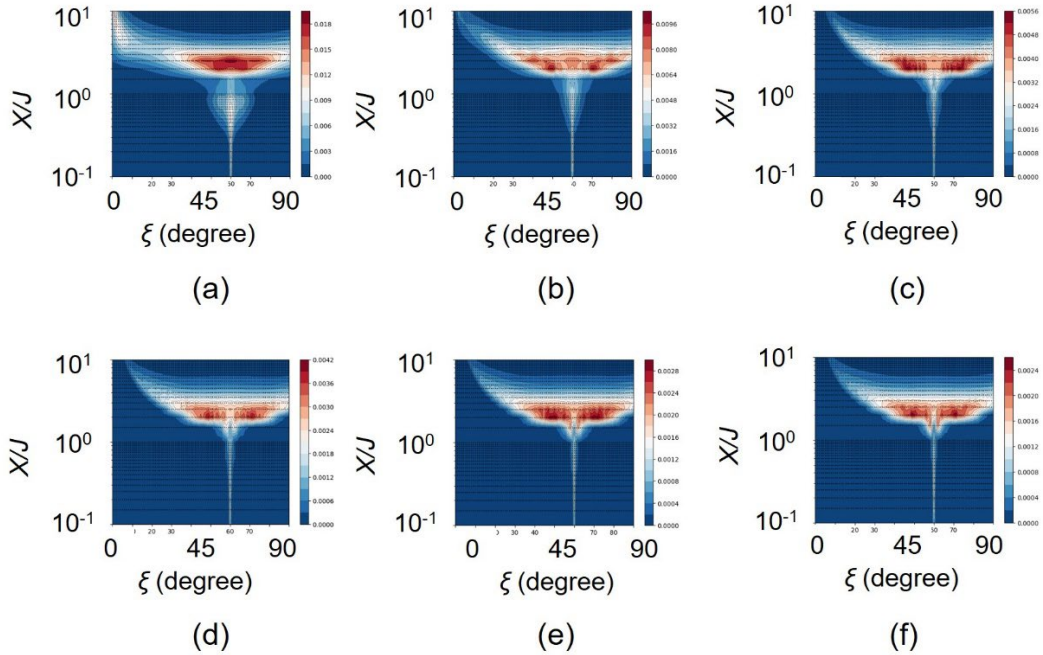(b)

(c)

(d)

(e)

(f)

14

Fig. 18 Dependence of P on ξ and χ/J in the case with DPP energy dissipation.

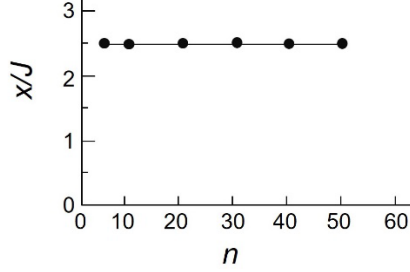(a) n =5, (b) 11, (c) 21, (d) 31, (e) 41, and (f) 51.

Fig. 19 Dependence of χ/J on n at which the integrated value of P takes the maximum value in the red belt in Fig. 18.

Figure 20 shows the dependence of P on ξ at the position χ/J =1 in Fig. 18. No bump on the curves is seen in this figure, which indicates that no interference takes place in the $T\{E\}(n)$, as was the case in Fig. 10. It was confirmed that these curves were symmetrical about ξ =60 degree, as was the case in Fig.15. Furthermore, the value of P in these figures takes the maximum P_{max} at $\xi = 60$ degree $(=(1/3)\pi$). Figure 21 shows the dependence of P_{max} on n. This figure shows that the value of P_{max} asymptotically approaches a constant value as n increases, from which it was confirmed that sufficiently high accuracy of approximation for the numerical calculation was obtained when $n \geq 51$, as was the case in Fig. 16. The value of P_{max} was 1×10^{-3} for $n \geq 51$, which is 10^{-1} times that in Fig. 16. This indicates that it is effective to suppress DPP energy dissipation (Case 1) at the slope of the $T_E(n)$ to increase the probability of DPP creation, as was described in Section 3. This indication is in agreement with the experimental results.
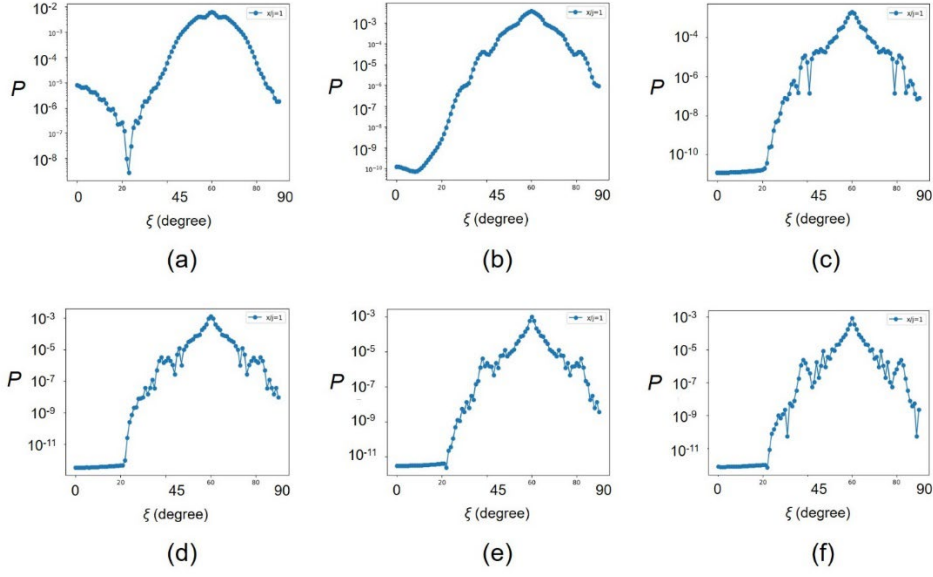
Fig. 20 Dependence of P on ξ at the position at $\chi / J = 1$ in Fig. 18.

(a) $n = 5$, (b) 11, (c) 21, (d) 31, (e) 41, (f) 51.
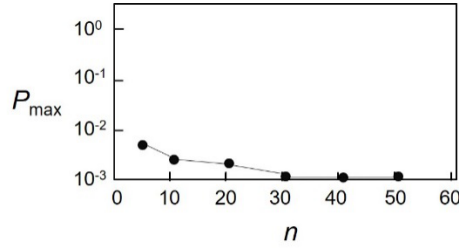

Fig. 21 Dependence of the maximum P_{max} on n.

Figure 22 shows the dependence of the ratio between the maximum P_{max} and the minimum P_{min} (of the curves in Fig. 20) on n. The curve in this figure also shows an asymptotic approach to a constant value, from which it was confirmed again that sufficiently high accuracy was obtained when $n \geq 51$.

It is found that the value of P_{max} in Fig. 21 is 1×10^{-3} for $n \geq 51$, which is smaller than the value 3×10^{-3} in Fig. 11. As with the discussion in Case 1, this smaller value indicates that the efficiency of DPP creation is lower for a smaller apex angle of the fiber probe, which is in agreement with the experimental results.
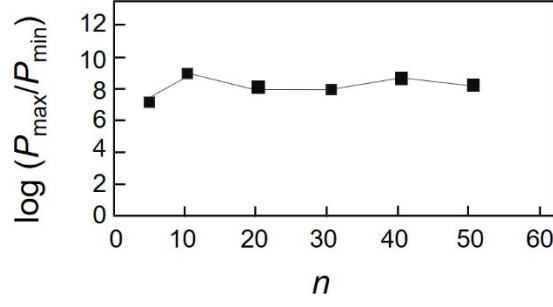
16

Fig. 22 Dependence of the ratio between the maximum P_{max} and minimum P_{min} on n.

5. Summary

To calculate the probability of DPP creation on the tip of a fiber probe on the basis of a QW model, the profile of the fiber probe was approximated by a two-dimensional right-angled isosceles triangle $T_{\mathrm{R}}(n)$ and an equilateral triangle $T_{E}(n)$. The calculations were carried out for cases without and with DPP energy dissipation at the slope of the triangular lattice. In both cases, the calculated maximum probability P_{max} converged to a constant value when $n \geq 51$, where n is the number n of the sites on the base of the triangle. This indicates that sufficiently high accuracy of the approximation above was obtained when $n \geq 51$.

Table 1 summarizes the calculated values of P_{max} for the physical parameter $\chi / J = 1$. This table shows that the value without DPP energy dissipation is larger than that with DPP energy dissipation, which is in agreement with experimental results. Furthermore, the value is larger for the $T_{\mathrm{R}}(n)$ (an apex angle of 90 degree) than that for the $T_{E}(n)$ (an apex angle of 60 degree), which is also in agreement with experimental results.

Table 1 Calculated values of P_{max} for $\chi / J = 1$.

	Right-angled isosceles triangle $T_{\mathrm{R}}(n)$	Equilateral triangle $T_{E}(n)$
Without DPP energy dissipation	3×10^{-1}	1×10^{-2}
With DPP energy dissipation	3×10^{-3}	1×10^{-3}

17

References

[1] M. Ohtsu, *Dressed Photons*, Springer, Heidelberg (2014).

[2] M. Ohtsu, "A Quantum Walk Model for Describing the Energy Transfer of a Dressed Photon," *Off-shell Archive* (September, 2021) OffShell: 2109R.001.v1., **DOI** 10.14939/2109R.001.v1

[3] M. Ohtsu, E. Segawa, and K.Yuki, "Numerical calculation of a dressed photon energy transfer based on a quantum walk model," *Off-shell Archive* (June, 2022) OffShell: 2206R.001.v1., **DOI** 10.14939/2206R.001.v1

[4] Y. Higuchi, M. Sabri, and E. Segawa, "Toward fixed point and pulsation quantum search on graphs driven by quantum walks with in- and out-flows: a trial to the complete graph", arXiv:2207.10633

[5] M. Ohtsu, *Off-shell Applications in Nanophotonics*, Elsevier, Amsterdam (2021), p.9.

[6] M. Ohtsu, *Near-Field Nano/Atom Optics and Technology*, Springer, Tokyo/Berlin (1998), pp.71-87.